Development of a High-SNR Stochastic sEMG Processor in a Multiple Muscle Elbow Joint

Handdeut Chang, *Member, IEEE*, Seulki Kyeong, Youngjin Na, Yeongjin Kim, and Jung Kim, *Member, IEEE*

***Abstract*— In the robotics and rehabilitation engineering fields, surface electromyography (sEMG) signals have been widely studied to estimate muscle activation and utilized as control inputs for robotic devices because of their advantageous noninvasiveness. However, the stochastic property of sEMG results in a low signal-to-noise ratio (SNR) and impedes sEMG from being used as a stable and continuous control input for robotic devices. As a traditional method, time-average filters (e.g., low-pass filters) can improve the SNR of sEMG, but time-average filters suffer from latency problems, making real-time robot control difficult. In this study, we propose a stochastic myoprocessor using a rescaling method extended from a whitening method used in previous studies to enhance the SNR of sEMG without the latency problem that affects traditional time average filter-based myoprocessors. The developed stochastic myoprocessor uses 16 channel electrodes to use the ensemble average, 8 of which are used to measure and decompose deep muscle activation. To validate the performance of the developed myoprocessor, the elbow joint is selected, and the flexion torque is estimated. The experimental results indicate that the estimation results of the developed myoprocessor show an RMS error of 6.17[%], which is an improvement with respect to previous methods. Thus, the rescaling method with multichannel electrodes proposed in this study is promising and can be applied in robotic rehabilitation engineering to generate rapid and accurate control input for robotic devices.**

***Index Terms*— Surface electromyography, decomposition, elbow, torque estimation, rescaling method.**

I. Introduction

SURFACE electromyography (sEMG) has been studied in many different fields, such as prosthesis or exoskeleton suit control [1], [2], clinical biomechanics [3], and ergonomics assessment. As a noninvasive method, sEMG can be used to represent muscle activation levels and estimate joint torque. The magnitude of sEMG shows a proportional relation to the muscle force because the magnitude of muscle force is mainly determined by the number of active motor units, their size (cross-sectional area), and their firing rate. However, this complex principle of sEMG introduces variability in joint torque estimation, and this variability impedes sEMG from being used as a stable control input of robotic devices. For this reason, many previous studies have utilized multiple sEMG features to generate stable control input. For example, Hudgins [4] used the slope sign change rate and zero crossing rate to classify previously defined tasks. However, a continuous torque estimator has been required to meet the increasing demand of torque control applications of recent robotic devices.

For the continuous estimation of joint torques using sEMG signals, various signal processing techniques have been proposed and applied in several areas. The most famous conventional method is rectification with a low-pass filtering algorithm to increase the signal-to-noise ratio (SNR). However, there exists a strong trade-off between the SNR and response time due to the phase delay induced by the low-pass filtering algorithm. The rapid response of the myoprocessor is significant if sEMG is utilized as a control input of robotic devices such as prostheses [1], [5] and exoskeleton suits [2], [6], [7], [8] because control input latency can induce severe instability and low performance problems. From previous studies [9], [10], [11], it is known that the sEMG signal typically precedes 50-100[ms] before the mechanical activity of muscle, which is called electromechanical delay (EMD). This suggests that the myoprocessor has to finish torque estimation within the EMD for high-performance robotic device control. For this reason, 100[ms] is treated as the standard latency (i.e., sampling time) of the myoprocessor in this study. In a previous study, Sanger [12] used a Bayesian filter to estimate torque by solving the Fokker-Planck partial differential equation for rapid response. However, this filter requires the model parameters and works only for previously defined motion.

To overcome the trade-off relation between the SNR and response time in the continuous torque estimation problem, multichannel electrode techniques have been introduced. Because the multichannel electrode uses the ensemble average instead of the time average, the SNR can be improved without loss of rapid response. Using 4-channel electrodes, Hogan [13], [14] proved that the maximum likelihood estimator of

Manuscript received 17 June 2022; revised 7 February 2023 and 17 April 2023; accepted 25 April 2023. Date of publication 8 June 2023; date of current version 14 June 2023. This work was supported by Incheon National University (International Cooperative) Research Grant in 2021. *(Handdeut Chang and Seulki Kyeong contributed equally to this work.) (Corresponding authors: Handdeut Chang; Yeongjin Kim.)*

This work involved human subjects or animals in its research. Approval of all ethical and experimental procedures and protocols was granted by the KAIST Institutional Review Board (IRB) under Approval No. KH2016-62.

Handdeut Chang and Yeongjin Kim are with the Department of Mechanical Engineering, Incheon National University, Incheon 22012, South Korea (e-mail: onemean@inu.ac.kr; Ykim@inu.ac.kr).

Seulki Kyeong is with the Department of Mechanical Engineering, Hannam University, Daejeon 34430, South Korea (e-mail: seulki.kyeong@hnu.kr).

Youngjin Na is with the Department of Mechanical Systems Engineering, Sookmyung Women's University, Seoul 04310, South Korea (e-mail: yjna@sookmyung.ac.kr).

Jung Kim is with the Korea Advanced Institute of Science and Technology, Daejeon 34141, South Korea (e-mail: jungkim@kaist.ac.kr).

Digital Object Identifier 10.1109/TNSRE.2023.3281410

the standard deviation of the sEMG signal is the root mean squared value (since the sEMG signal follows a zero-mean Gaussian distribution [15]) and experimentally demonstrated that the SNR can be improved by a novel signal whitening method. Because the whitening method makes the magnitudes of uncorrelated sEMG signals equal (i.e., small sEMG signals can be amplified), this method has been utilized in many previous studies [16], [17], [18], [19], [20], [21] to improve the SNR. However, the whitening method theoretically assumes that a muscle consists of independent muscle units of equal sizes, which means that the anatomical structure of the muscles is not taken into account. Furthermore, activation of deep muscles, which is difficult to measure by sEMG devices, has not been considered to estimate joint torque. In a previous study, Staudenmann [22] used 7-channel sEMG and demonstrated that appropriate placement of electrodes could reduce interference from the biceps brachii (superficial muscle) and make it possible to assess the activation of the brachialis (deep muscle) with sEMG.

Inspired by these previous results, in this study, we propose a simple new torque estimation algorithm, named the rescaling method. The developed algorithm is less sensitive to the location of the electrode but shows higher SNR than conventional algorithms because it utilizes multiple electrodes distributed all over the multiple muscles with a simple calibration step to measure the independent muscle unit signals and estimate joint torque. The rescaling method assumes that each muscle, including deep muscles, is split into independent compartments (called the muscle units in this study). Additionally, it is assumed that the activation of each muscle unit is linearly proportional to the contraction force of the muscle unit. Based on these two assumptions, the proposed rescaling method introduces two parameters: a linearizing factor and a rescaling factor. Using these two parameters, the torque estimation error with respect to the reference torque sensor is minimized, which contributes to a high SNR. The performance of the proposed method is evaluated with respect to dynamic elbow flexion torque estimation in isometric conditions (i.e., multiple muscle joints) and compared to other joint torque estimation methods, such as moving average and whitening. Additionally, the physiological and anatomical meaning of the rescaling method is discussed.

II. Joint Torque Estimation Method

A. Model of the Stationary sEMG Signal

The sEMG signal results from the spatial and temporal superposition of the motor unit action potentials within the detection region of the electrode. An analytical model of the sEMG signal is difficult to obtain because of its stochastic property (i.e., timing of each action potential, different muscle unit sizes, and the location of an electrode on skin). For this reason, in this paper, we use a stochastic model of sEMG signals to estimate muscle activation. The stochastic model of sEMG was first investigated in detail by Clancy [15]. He suggested that the sEMG signal is a stochastic signal whose probability density function can be expressed as a

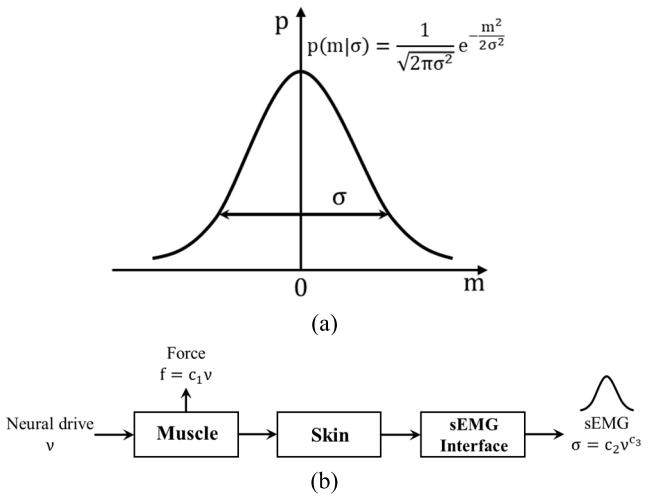

Fig. 1. (a) Conditional probability density function of a stationary sEMG signal (zero-mean Gaussian distribution). (b) Concepts of the neural drive, muscle force and sEMG models. c_i is a constant.

Gaussian (normal) distribution of which the mean value is always 0, as shown in **Fig. 1**-(a). Then, the conditional probability density function of the sEMG signal can be expressed as follows:

$$P(m \mid \sigma) = \frac{1}{\sqrt{2\pi\sigma^2}} e^{-\frac{m^2}{2\sigma^2}} \tag{1}$$

where m is the measured sEMG signal sample and σ is the population standard deviation of the sEMG signal. It is assumed that muscle activation does not vary with time evolution (i.e., the sEMG signal is a stationary random process). (1) indicates the prior probability that the sEMG signal is measured as m under the condition that the population standard deviation is given as σ. Since the mean value of the sEMG signal is always 0 and independent of muscle activation, the standard deviation σ in (1) is the only parameter of muscle activation. Thus, the estimation of the population standard deviation σ is related to the estimation of muscle activation, and muscle activation is generally observed as a nonlinear function of σ in most previous studies. Therefore, in this paper, we assume that σ represents distorted muscle activation due to the sEMG interface, that the neural drive ν is a nonlinear function of σ, and that the muscle force f is a linear function of ν. In this assumption, σ should be estimated first in order to estimate the neural drive ν and muscle force f (see **Fig. 1**(b)).

To statistically estimate the population standard deviation σ from the measured sEMG signal m, maximum likelihood estimation can be used. The maximum likelihood estimator for a Gaussian distribution can be obtained by two different methods. One is the time average $\bar{\sigma}$ calculated using time series data from a fixed i-th electrode, and the other is the ensemble average $\hat{\sigma}$ using ensemble data from multiple electrodes at fixed time t.

Time average:

$$\bar{\sigma}(i) = \sqrt{\frac{1}{\tau}\int_0^{\tau} m_i^2(t)dt} \tag{2}$$

Ensemble average:

$$\hat{\sigma}(t) = \sqrt{\frac{1}{N-1}\sum_{i=1}^{N} m_i^2(t)} \tag{3}$$

where $m_i(t)$ is the sEMG signal of the i-th electrode at time t, τ is the time record length (sampling time), and N is the total number of electrodes. These two estimates are theoretically equal in the case of an ergodic signal [24]. Estimating the population standard deviation σ via the time average $\bar{\sigma}$ has the advantage that a large number of samples for accurate estimation can be acquired easily, but this requires a large time record length, which induces a time delay of the signal processor (i.e., a low-pass filter). On the other hand, the ensemble average $\hat{\sigma}$ does not induce time delay because it collects more data from more electrodes without time delay. However, ensemble averaging also has limitations because electrodes cannot be added arbitrarily due to limited space to allocate the electrodes on the surface of the skin. Thus, in this study, both the ensemble average $\hat{\sigma}$ and the time average $\bar{\sigma}$ are used as the maximum likelihood estimators to improve the estimation accuracy of the population standard deviation σ. Then, the expectation and variance of each estimate are given as follows [24]:

Time average:

$$E\left[\bar{\sigma}^2\right] = \sigma^2, \; V\left[\bar{\sigma}^2\right] \approx \frac{2\sigma^4}{B\tau} \tag{4}$$

Ensemble average:

$$E\left[\hat{\sigma}^2\right] = \sigma^2, \; V\left[\hat{\sigma}^2\right] = \frac{2\sigma^4}{N-1} \tag{5}$$

where B is the sampling bandwidth of the signal. From (4) and (5), the expectations of both $\bar{\sigma}^2$ and $\hat{\sigma}^2$ are equal to the population variance σ^2, which implies unbiased estimators. To obtain an accurate estimation of σ, the variance of estimates (i.e., $V\left[\bar{\sigma}^2\right]$ and $V\left[\hat{\sigma}^2\right]$) should be minimized. According to (4) and (5), the sampling bandwidth B and the number of electrodes N should be maximized to minimize the variance of estimates if the tolerable time delay of the processor is given (i.e., the maximum τ is given). From previous research [25], the effective bandwidth of the sEMG signal is approximately known as 0.5 [kHz], which requires just a 1.0 [kHz] sampling rate as a result of the Nyquist sampling theorem. The number of electrodes N is selected as 16 by considering muscle size and limited space on skin. Thus, in this study, sEMG data are sampled from 16 electrodes at a 1.0 [kHz] sampling rate.

The relation in (4) and (5) clearly shows that variances of $\hat{\sigma}^2$ and $\bar{\sigma}^2$ are proportional to the square of the population variance σ^2 (i.e., σ^4) and inversely proportional to the sampling bandwidth B, time record length τ and number of electrodes N. This means that the estimation accuracy of σ drops with increasing muscle activation and decreasing number of electrodes and time record length τ. Because a long record length τ can induce a time delay, the use of multichannel electrodes ($N > 1$) can play a significant role in increasing the estimation accuracy with minimal time delay.

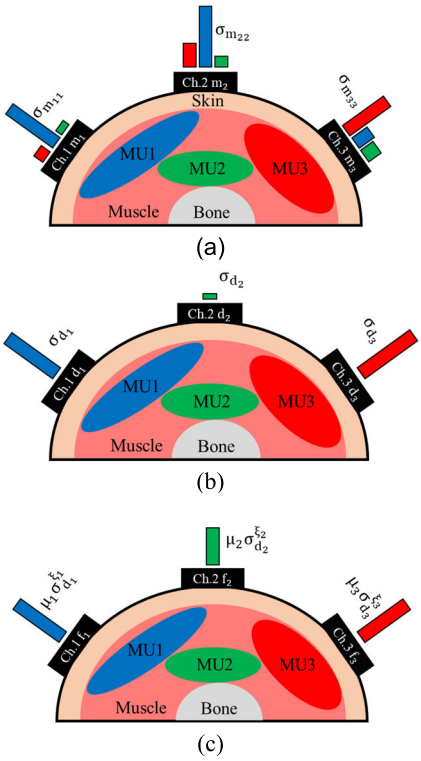

Fig. 2. Concept of muscle unit decomposition and rescaling method. (a) Correlated sEMG signals m_i. (b) Independent sEMG signals d_i. (c) Rescaled muscle unit force signals f_i.

B. Muscle Unit Decomposition

To estimate the population standard deviation σ using ensemble samples, independence between electrodes should be satisfied. However, it is difficult to obtain independent sEMG data in practice because sEMG signals depend on the location of the electrode. In the case of a Gaussian distribution, an uncorrelated sample is equivalent to an independent sample. Thus, as in previous studies [13], [14], uncorrelated sEMG signals $d_i(t)$ can be extracted from the correlated sEMG signals $m_i(t)$. As shown in **Fig. 2**-(a), each electrode on the skin receives a sum of the action potentials of muscle units (MUs). However, this sum can be distorted because the distances from an electrode to different muscle units may be different. To investigate this, the $\mathbb{R}^{N\times N}$ covariance matrix $\mathbf{C}_m$ among electrodes can be calculated as follows:

$$\mathbf{C}_m = \begin{bmatrix} \sigma^2_{m_{11}} & \cdots & \sigma^2_{m_{1\,N}} \\ \vdots & \ddots & \vdots \\ \sigma^2_{m_{N1}} & \cdots & \sigma^2_{m_{NN}} \end{bmatrix}, \sigma^2_{m_{ij}} = E\left[m_i m_j\right] \tag{6}$$

In (6), the diagonal elements (i.e., $\sigma^2_{m_{ii}}$) are the squares of the estimated standard deviations from the i-th electrode, and the nondiagonal elements (i.e., $\sigma^2_{m_{ij}}$) are the covariances between the i-th and j-th electrodes and generally take nonzero values, which means that the two corresponding channels are mutually correlated. To extract uncorrelated signals, the eigenvalue decomposition technique is used. As a result, the eigenvalue and eigenvector matrix can be derived

from $\mathbf{C}_m$ as follows:

$$\mathbf{C}_m = \mathbf{V}^{-1}\mathbf{\Lambda}\mathbf{V}$$
$$\mathbf{C}_m = \begin{bmatrix} v_{11}^2 & \cdots & v_{1\,N} \\ \vdots & \ddots & \vdots \\ v_{N1}^2 & \cdots & v_{NN} \end{bmatrix}, \mathbf{\Lambda} = \begin{bmatrix} \lambda_1^2 & & 0 \\ & \ddots & \\ 0 & & \lambda_N^2 \end{bmatrix} \tag{7}$$

where $\mathbf{V}$ and $\mathbf{\Lambda}$ are the $\mathbb{R}^{N\times N}$ eigenvector and eigenvalue matrices, respectively. $\mathbf{V}$ is physically related to the locations of the electrodes, and independent sEMG signals can be extracted using this information. Using this eigenvector matrix $\mathbf{V}$, the independent sEMG signal $\mathbf{d}(t)$ is obtained as follows:

$$\mathbf{d}(t) = \mathbf{V}\mathbf{m}(t)$$
$$\begin{bmatrix} d_1(t) \\ \vdots \\ d_N(t) \end{bmatrix} = \begin{bmatrix} v_{11} & \cdots & v_{1\,N} \\ \vdots & \ddots & \vdots \\ v_{N1} & \cdots & v_{NN} \end{bmatrix} \begin{bmatrix} m_1(t) \\ \vdots \\ m_N(t) \end{bmatrix} \tag{8}$$

It is assumed that eigenvector $\mathbf{V}$ is a constant (i.e., time-invariant) matrix regardless of the muscle activation level if the location of electrodes is fixed. The validity of this assumption is experimentally demonstrated in section III. From an engineering point of view, this assumption is significant because if the eigenvector is a function of muscle activation, an infinite number of eigenvector matrices with respect to every muscle activation level is required to obtain an independent sEMG signal $\mathbf{d}(t)$. Then, the $\mathbb{R}^{N\times N}$ covariance matrix $\mathbf{C_d}$ between $d_i(t)$ and $d_j(t)$ can be calculated as follows:

$$\mathbf{C}_d = \begin{bmatrix} \sigma_{d_1}^2 & & 0 \\ & \ddots & \\ 0 & & \sigma_{d_N}^2 \end{bmatrix}, \quad \sigma_{d_i}^2 = E[d_i d_i] \tag{9}$$

Because the autocovariance $\sigma_{d_i}^2$ (i.e., square of eigenvalue λ_i) corresponds to the square of independent sEMG d_i, $\mathbf{C_d}$ becomes a diagonal matrix. However, it should be noted that σ_{d_i} does not contain true magnitude information of the i-th muscle unit because sEMG signals are the result of distortion due to different fat layer thicknesses between muscle units and electrodes (see **Fig. 2**-(b)). For this reason, many previous studies [23], [26], [27], [28], [29] have reported that the relationship between muscle force and the standard deviation of the sEMG signal σ is not always linear. Thus, based on a previous study [29], the muscle force is assumed to be a power function of σ_{d_i} in this study, as follows:

$$F(t) = \sum_{i=1}^{n} f_i(t) = \sum_{i=1}^{n} \mu_i v_i(t) = \sum_{i=1}^{n} \mu_i \sigma_{d_i}^{\xi_i}(t) \tag{10}$$

where F is the muscle force, v_i is the neural drive of the i-th muscle unit, f_i is the force of the i-th muscle unit, and μ_i and ξ_i are rescaling and linearizing constants, respectively, to compensate for the distances between the electrodes and muscle units (see **Fig. 2**-(c)). However, in practice, it is difficult to obtain μ_i and ξ_i from the muscle model because they vary with anatomical muscle conditions and electrode patterns. This physical limitation originates from the fact that sEMG signals have to be measured on the surface of the skin rather than inside the muscle. Therefore, in this paper, a calibration procedure under isometric conditions is used in practice to obtain μ_i and ξ_i. The method is explained in the next section.

C. Rescaling Method Under Isometric Conditions

The total joint torque T, which is generated by n synergist muscles, can be simply modeled as follows [30]:

$$T(\theta, \dot{\theta}, \sigma_{d_i}) = \sum_{i=1}^{n} T_i = \sum_{i=1}^{n} r_i f_i \tag{11}$$

where T is the net joint torque, and r_i and f_i are the length of the moment arm and the force of the i-th muscle, respectively. Physiologically, it is well known that the muscle force is a function of the joint angle θ, angular velocity $\dot{\theta}$ and muscle activation σ_{d_i} (i.e., $f_i = f_i(\theta, \dot{\theta}, \sigma_{d_i})$). However, if isometric conditions are assumed (i.e., θ, $\dot{\theta}$ and r_i are constant), then the joint torque T depends solely on muscle activation, which means that this torque can be estimated from sEMG data (muscle activation) as follows:

$$\hat{T}(\sigma_{d_i}) = \sum_{i=1}^{n} r_i f_i = \sum_{i=1}^{n} r_i \mu_i v_i = \sum_{i=1}^{n} \gamma_i \sigma_{d_i}^{\xi_i} \tag{12}$$

where $\hat{T}$ is the estimated torque, and $\gamma_i = r_i\mu_i$ is a positive constant. From (12), it can be considered that σ_{d_i} is decomposed from the measured sEMG signal and that $v_i = \sigma_{d_i}^{\xi_i}$ represents muscle activation (i.e., neural drive), which compensates for the distortion of the sEMG signal. In (12), γ_i and ξ_i can be estimated because the joint torque T and σ_{d_i} can be measured by a torque sensor and from the sEMG signal, respectively. However, γ_i and ξ_i cannot be uniquely determined by T and σ_{d_i}. Therefore, in this study, γ_i and ξ_i are determined such that the torque estimation error ε between the measured torque T and the torque $\hat{T}$ estimated in the calibration step is minimized, as follows:

$$\min\left[\varepsilon^2\right] = \frac{E\left[(\hat{T} - T)^2\right]}{T^2} = \frac{E\left[\left(\sum_{i=1}^{n} \gamma_i \sigma_{d_i}^{\xi_i} - T\right)^2\right]}{T^2} \tag{13}$$

The rescaling procedure in this study has the advantage of estimating joint torque, which is generated by several synergist muscles. For example, human elbow flexion torque is mainly generated by two muscles. One is the biceps brachii, which is located near the surface of the skin, and the other is the brachialis, which is located deep under the biceps. Muscle unit activation signals from the brachialis are easily diminished on their way to the surface of skin, making it difficult to estimate the activation of the brachialis. However, the rescaling procedure can be used to reconstruct the original magnitude of deep muscle unit activation.

D. Noise Reduction Algorithm

It is important to suppress noise from the power line and motion artifacts to improve the estimation accuracy of σ. In general, a notch filter with a bandstop frequency of 60 [Hz] and a high-pass filter with a cutoff frequency of 20 [Hz] are

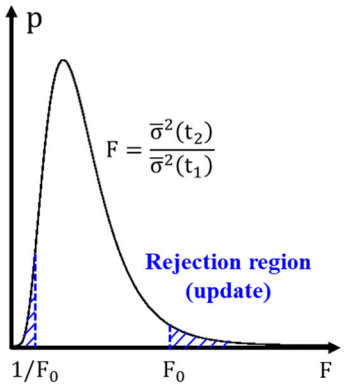

Fig. 3. Nonstationary sEMG signal estimation. The F test rejects the null hypothesis $\bar{\sigma}^2(t_1) = \bar{\sigma}^2(t_2)$, indicating that $\bar{\sigma}^2(t)$ should be updated, if $F > F_0$ or $F < 1/F_0$.

used to reduce the effects of power line noise and motion artifacts, respectively. However, these two filters cannot remove all baseline noise, which can appear even when muscles are not activated. Thus, the sEMG signal m_i can be modeled as follows:

$$m_i(t) = s_i(t) + n_i(t) \tag{14}$$

where the index i denotes the electrode number, m_i is the measured sEMG signal contaminated by noise, s_i is the pure sEMG signal, and n_i is noise. Then, the covariance between sEMG signals m_i and m_j can be calculated as follows:

$$E\left[m_i m_j\right] = E\left[s_i s_j\right] + E\left[n_i n_j\right] \rightarrow \sigma^2_{m_{ij}} = \sigma^2_{s_{ij}} + \sigma^2_{n_{ij}} \tag{15}$$

where $\sigma^2_{m_{ij}}$ is the measured sEMG covariance, $\sigma^2_{s_{ij}}$ is the pure sEMG covariance, and $\sigma^2_{n_{ij}}$ is the noise covariance between the two electrodes. It is assumed that the noise n_i and pure sEMG s_i are mutually uncorrelated. From (4), the pure sEMG covariance can be expressed in matrix form as follows:

$$\mathbf{C}_s = \begin{bmatrix} \sigma^2_{s_{11}} & \cdots & \sigma^2_{s_{ij}} \\ \vdots & \ddots & \vdots \\ \sigma^2_{s_{ji}} & \cdots & \sigma^2_{s_{NN}} \end{bmatrix}, \quad \sigma^2_{s_{ij}} = \sigma^2_{m_{ij}} - \sigma^2_{n_{ij}} \tag{16}$$

The noise covariance $\sigma^2_{n_{ij}}$ can be experimentally obtained from sEMG data measured when the muscle is not activated (i.e., $\sigma^2_{m_{ij}} = \sigma^2_{n_{ij}}$ if $\sigma^2_{s_{ij}} = 0$). Thus, a pure sEMG signal can be theoretically extracted from sEMG measurements. This result shows the advantage of the stochastic sEMG processor in noise reduction compared with traditional time domain approaches such as low-pass filter algorithms.

E. Nonstationary sEMG Signal Estimation

The methods mentioned in the previous sections are valid only if the sEMG signal is a stationary process, which means that the muscle torque does not vary with time evolution; $\sigma^2(t)$ is constant. However, the sEMG signal becomes a nonstationary process if muscle torque dynamically varies with time evolution; $\sigma^2(t)$ is time varying. To estimate the time-varying population variance $\sigma^2(t)$, the method of analysis of variance (i.e., F test) is used in this study (see **Fig. 3**).

First, it is assumed that there are two different variances $\bar{\sigma}^2(t_1)$ and $\bar{\sigma}^2(t_2)$ which are estimated by the time average in Table II at different times $t_1 < t_2$ as follows:

$$\bar{\sigma}^2(t_1) = \frac{1}{\tau}\int_{t_1-\tau}^{t_1} m^2(t)dt,$$
$$\bar{\sigma}^2(t_2) = \frac{1}{\tau}\int_{t_2-\tau}^{t_2} m^2(t)dt \tag{17}$$

Then, a null hypothesis that $\bar{\sigma}^2(t_2)$ is identical to $\bar{\sigma}^2(t_1)$ can be developed. To test this hypothesis, a new variable F can be introduced as follows:

$$\frac{1}{F_0} > F = \frac{\bar{\sigma}^2(t_2)}{\bar{\sigma}^2(t_1)} > F_0 \tag{18}$$

F_0 is a constant that determines the significance level. According to the F test, F follows the F distribution with $(n-1, n-1)$ degrees of freedom, and the null hypothesis is rejected if the inequality in (18) is satisfied. By setting an appropriate level of significance F_0, $\bar{\sigma}^2(t)$ can be updated in real time with high accuracy. The advantage of the F test is improving the SNR by preventing uncertain updates. The accuracy of the F test can be increased by collecting a large number of samples n because this makes it easier to reject the null hypothesis with respect to the same level of significance F_0, but doing so can also induce a long estimation delay (i.e., there is a trade-off between delay and accuracy). Thus, in this study, taking into account the human EMD, F_0 is set to 1.4 with 100 samples, which corresponding to the 5 [%] significance level (i.e., $p < 0.05$). Note that this accuracy is obtained when a single electrode is used alone. In this study, 16 electrodes are utilized to collect more samples within the same time to improve the SNR, which is the reason why multichannel electrodes play a significant role in this study. **Fig. 4** shows the overall torque estimation algorithm proposed in this study.

III. Experimental Methods

A. Experimental Setup

For this study, 15 healthy subjects (10 males and 5 females) who had no previous experience in our experiments were recruited. The subjects were encouraged to generate a torque profile by following visual feedback of the desired torque profile, which was displayed on a monitor (see **Fig. 5**-(a)). The desired torque profiles were trapezoidal functions with 4 [s] static contractions and 2 [s] ascending/descending contractions with respect to 7 linearly increasing torque levels (i.e., level 1 is 11.4 [%] and level 7 is 80[%] of the maximum voluntary contraction torque) and free force-varying contractions under isometric conditions. To prevent muscle fatigue, 3 [s] rest time was given between contractions.

sEMG signals were measured while the subjects performed elbow flexion. The upper arm was tightly fixed in a custom-made brace, and the elbow and shoulder joint angles were fixed at 135 [°] and 90 [°], respectively. Four cross-shaped 4-channel electrodes (dEMG sensors, Delsys, USA) were used as sEMG sensors to collect sEMG samples (i.e., a total of 16 electrodes). As shown in **Fig. 5**-(b), sensors 1 and 2 were located over the

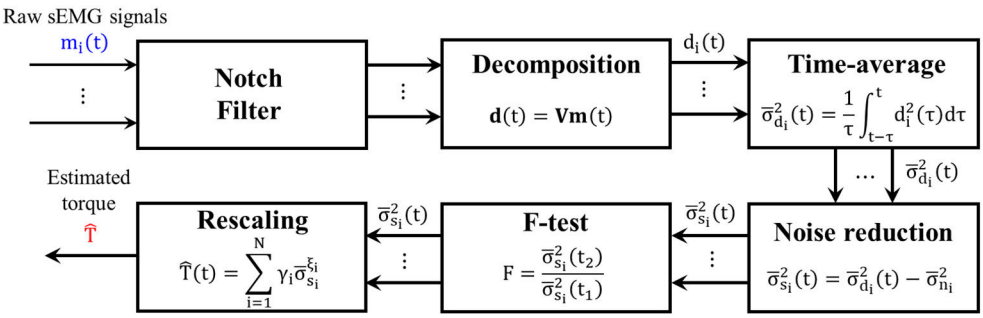

Fig. 4. The overall algorithm for joint torque estimation.

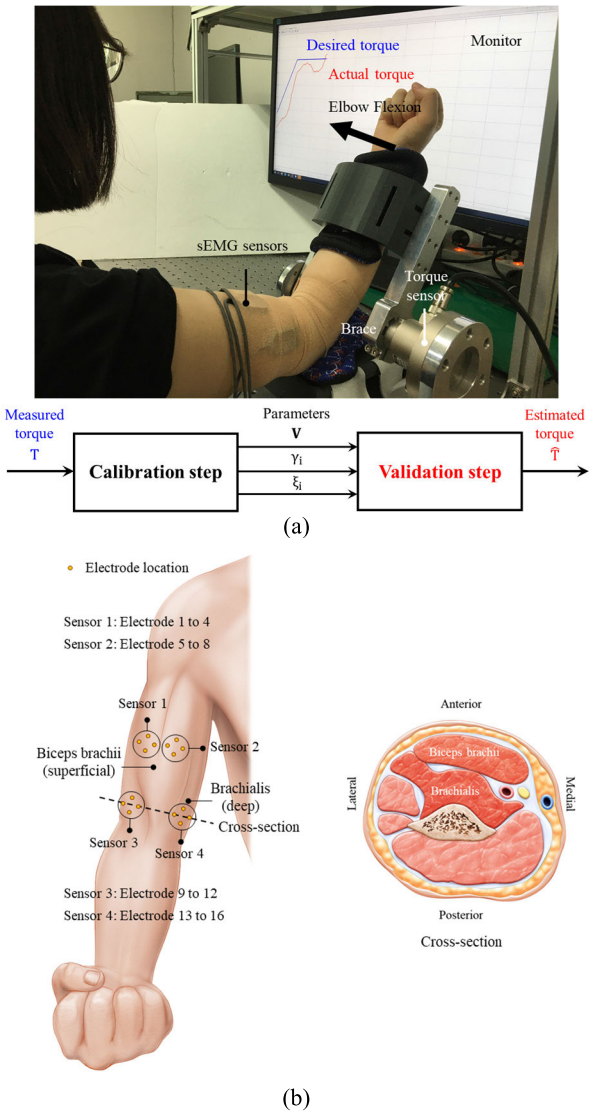

Fig. 5. (a) Experimental setup and procedure (b) Electrode locations over biceps brachii and brachialis, and cross-section of muscles.

proximal part of the long and short head of the biceps brachii. Sensors 3 and 4 were located over the medial and lateral sides of the distal upper arm where the brachialis muscle becomes close to the skin (see **Fig. 5**-(b)) [22]. The ground electrode was attached to the elbow joint of the left arm. The elbow flexion torque was measured by a torque sensor (TCN16-20K, Dacell, Korea), and the torque sensor signal was sampled at 1.0 [kHz]. The sEMG signals were also sampled at 1.0 [kHz] and high-pass filtered with a 20 [Hz] cutoff frequency, and a notch filter was utilized to eliminate 60 [Hz] power line noise [32].

B. Experimental Procedure

The experimental procedure involved two main steps: the calibration step and the validation step. At the beginning of the calibration step, the subjects were asked to generate the maximum elbow flexion torque in order to measure the maximum voluntary contraction torque. Then, the subjects were asked to produce elbow flexion torque following the profile displayed on the monitor. After the experiment was finished, the eigenvector matrix $\mathbf{V}$ was extracted from the covariance matrix $\mathbf{C}_m$ to be decomposed into 16 independent sEMG signals. Although it is assumed that $\mathbf{V}$ is a constant matrix, it may change slightly in practice depending on the torque level. Therefore, the 4th torque level data among the 7 torque levels (i.e., 50[%] of the maximum voluntary contraction torque) were used to calculate $\mathbf{C}_m$ to minimize the changes in $\mathbf{V}$ among the torque levels.

Then, the independent muscle unit signals d_i were calculated using (8), and the standard deviation of each independent muscle unit σ_{di} was obtained using an equation analogous to Table II with an averaging time of 100 [ms]. Because σ_{d_i} contains a noise component σ_{n_i}, the pure signal σ_{s_i} was extracted from (16). Subsequently, the nonlinear index ξ_i was estimated via the nonlinear regression method to maximize the correlation (i.e., linearity) between T and the sum of $\sigma_{s_i}^{\xi_i}$ by using the mean values at each of the 7 static torque levels. Finally, the γ_i that would minimize the torque estimation error ε in (13) was calculated to complete the calibration step.

In the validation step, the subjects were also asked to produce elbow flexion torque as in the calibration step, but the torque was estimated online by using the parameters γ_i, ξ_i, and $\mathbf{V}$ obtained in the calibration step. Finally, the torque estimation error ε in (13) and the SNR were validated.

IV. Experimental Results

A. Experimental Results

Fig. 6 shows the raw sEMG data m_i of subject 1. The sEMG signals from channels 1 to 8, which are located over the biceps brachii, and the signals from channels 9 to 16, which are

TABLE I
PARAMETERS USED IN THE STOCHASTIC sEMG PROCESSOR FOR SUBJECT 1

Parameters	Values															
γ_i	0.8	0.2	2	2	1	3	0.4	4	1	0.4	0.3	0.3	0	0	0	0
ξ_i	0.39	0.47	0.54	0.51	0.49	0.57	0.41	0.86	0.73	0.68	0.70	0.80	0	0	0	0

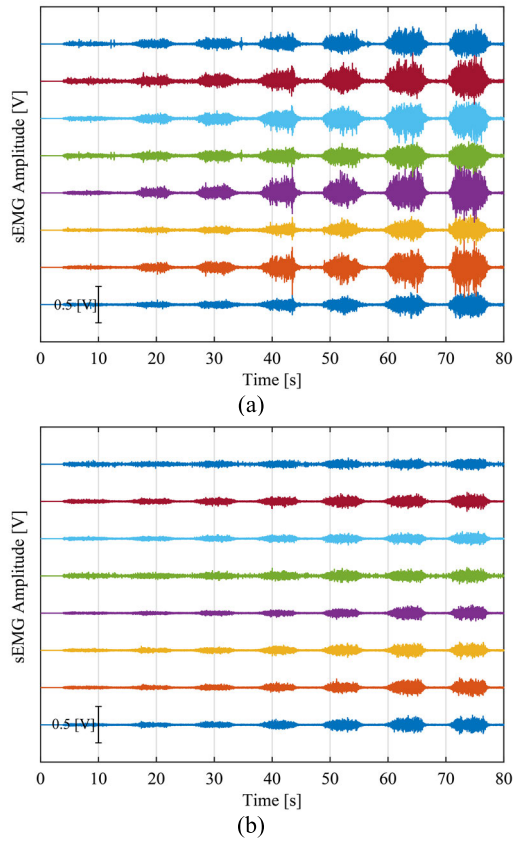

Fig. 6. Measured raw sEMG data m_i of subject 1. (a) Signals from electrodes numbered 1 to 8 (Biceps brachii). (b) Signals from electrodes number 9 to 16 (Brachialis).

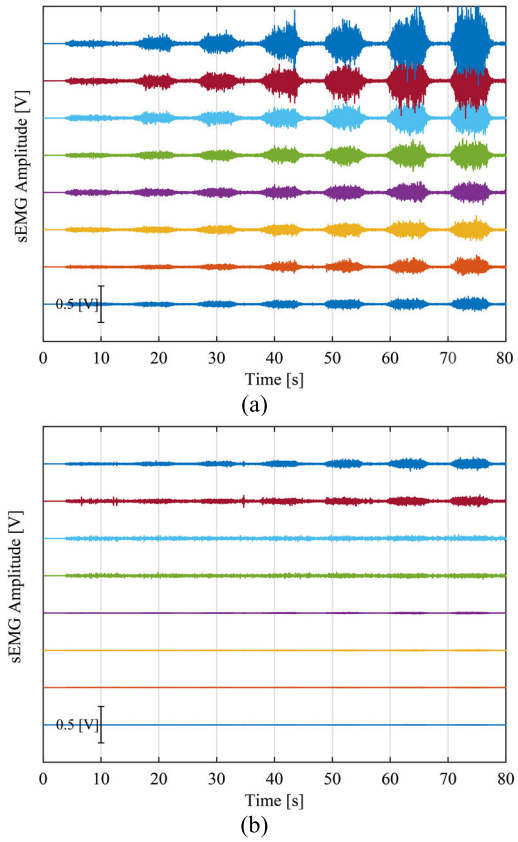

Fig. 7. Decomposed independent sEMG data d_i of subject 1. (a) The 8 signals with higher amplitudes. (b) The 8 signals with lower amplitudes.

located over the brachialis, are shown in **Fig. 6**-(a) and (b), respectively. **Fig. 7** shows the decomposed independent sEMG data d_i of subject 1, which were calculated from m_i using $\mathbf{V}$. These 16 d_i signals are labeled by the size of the eigenvalues. $\mathbf{V}$ was extracted from torque level 4 (middle) resulting in the smallest correlations at torque levels 1 (lowest) and 7 (highest). **Table I** shows the parameters estimated in the rescaling procedure. Using these parameters, the relationships between the measured torque T and the standard deviation of d_i (i.e., σ_{d_i}) were linearized. Finally, **Fig. 8** shows the experimental results in the validation step. In **Fig. 8**-(a), the blue curve shows the result of the rescaling method in this study, while the gray and yellow curves show the results of the moving average filter and the whitening method proposed in previous studies [1], [14], [17]. The sampling time was fixed to 100[ms] to ensure that the latency of each myoprocessor would be identical and to compare the RMS error. **Fig. 8**-(b) shows an enlarged version of **Fig. 8**-(a) for torque level 4. The averaged RMS error with respect to the maximum voluntary contraction torque in each experiment in **Fig. 8** is calculated and summarized in **Table II**. The calculated average RMS error is 6.17 [%] (male: 4.59 [%], female: 9.32 [%]), representing an improvement over the results of the two conventional algorithms (P-values are significant according to the t-test. $^{***}p \leq 0.001$). **Fig. 8**-(a) shows the results for free force-varying (dynamic) contractions under isometric conditions. Similarly, the proposed rescaling method (the blue curve) shows the least RMS error.

In **Fig. 9**-(a), the blue curve shows the result of the proposed 16 channels (i.e., biceps brachii and brachialis) with the rescaling method in this study, while the other curves show the results of the case in which only 1, 4 and 8 channels are used (i.e., biceps brachii only with the rescaling method). **Fig. 9**-(b) shows an enlarged version of **Fig. 9**-(a) for torque level 4. As shown in the figure, the RMS error decreases as the number of electrodes increases (i.e., gray, green, yellow curve). Furthermore, the figure shows that additional electrodes located over the brachialis can further improve the RMS error. However, the results also show that the efficiency

TABLE II
EXPERIMENTAL RESULTS

Subject number	Male/ Female	Averaged RMS error (% MVC)		
		Rescaling	Whitening	MAV
1	Male	3.67	10.84	18.07
2	Male	5.61	12.09	15.27
3	Male	3.51	6.05	14.51
4	Male	5.34	13.18	15.81
5	Male	4.34	9.05	14.70
6	Male	3.23	5.61	11.44
7	Male	3.77	6.75	14.67
8	Male	7.23	12.43	13.96
9	Male	3.50	6.82	10.59
10	Male	5.70	9.38	15.08
11	Female	12.55	18.34	22.86
12	Female	6.41	14.32	18.82
13	Female	11.58	20.01	24.25
14	Female	9.81	21.21	19.24
15	Female	6.24	19.68	17.62
Male		4.59 ± 1.25	9.22 ± 2.68	14.41 ± 2.01
Female		9.32 ± 2.60	18.71 ± 2.38	20.56 ± 2.54
Total		6.17 ± 2.87	12.38 ± 5.16	16.46 ± 3.64

of the additional electrode is decreased and almost saturated with 8 channels on the biceps brachii (see the green and blue curves). **Fig. 10** summarizes the experimental results with respect to the RMS error of subject 1. The rescaling method with 16 electrodes shows the most accurate torque estimation results. These results are discussed further in the next section.

V. DISCUSSIONS

A. sEMG-Torque Relationship and Rescaling Method

In this study, we assume that the joint torque T and neural drive ν have a linear relationship, which can be distorted in the process of measuring the neural drive on the skin surface as a form of sEMG σ. To compensate for this distortion and estimate the neural drive, a rescaling method is proposed. In previous studies, the relationship between the standard deviation of the sEMG signal and the force has been determined to exhibit both linear and nonlinear relationships. Woods [33] reported that a linear relationship between sEMG and torque was found in the pollicis and soleus, while a nonlinear relationship was found in the biceps and triceps. Bigland [34] reported that a linear relationship can be found in muscles that control the fingers. However, Lawrence [23] reported that the relationship is closer to a parabolic shape in other muscles. Furthermore, Fuglevand [35] performed a simulation study and found that the relationship can vary depending on the recruitment strategy (narrow or broad range) and uniformity among the peak firing rates of the different motor units, and Farina [36] also showed that the sEMG-force relationship can vary depending on the locations of the motor units. From the results of previous studies, therefore, it is considered that the characteristics of the target muscle generally influence the relationship between sEMG and torque, and this relationship is difficult to generalize. In this study, we also found a nonlinear relationship between sEMG and torque. This relationship is shown at the muscle unit level (i.e., decomposed sEMG d_i),

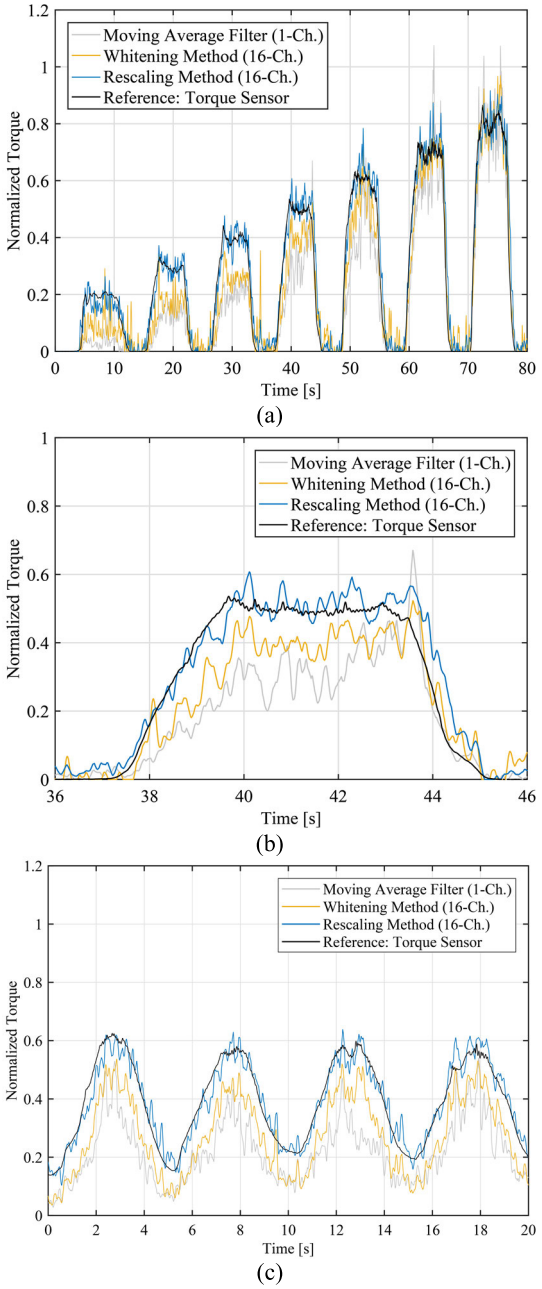

Fig. 8. The results of the validation step (subject 1). (a) Experimental results with respect to different torque estimation algorithms. (b) Torque estimation results on torque level 4. (c) Dynamic torque estimation results (sinusoidal function).

as shown in **Fig. 11**-(a). In most subjects, the standard deviation of relatively strong muscle units (e.g., σ_{d_1} and σ_{d_2}) shows a nonlinear relationship with respect to joint torque, while other muscle units show an almost linear relationship. In this paper, this nonlinear relationship is corrected to a linear relationship, and the neural drive is estimated via the rescaling method, as shown in **Fig. 11**-(b). As a result, the error between the estimated and measured torque can be minimized.

The rescaling method introduced in this study can be used to estimate the signal sources of the muscle units. In **Fig. 11**, the shapes of the markers indicate the estimated origins of the muscle units; circles indicate the brachialis, and triangles

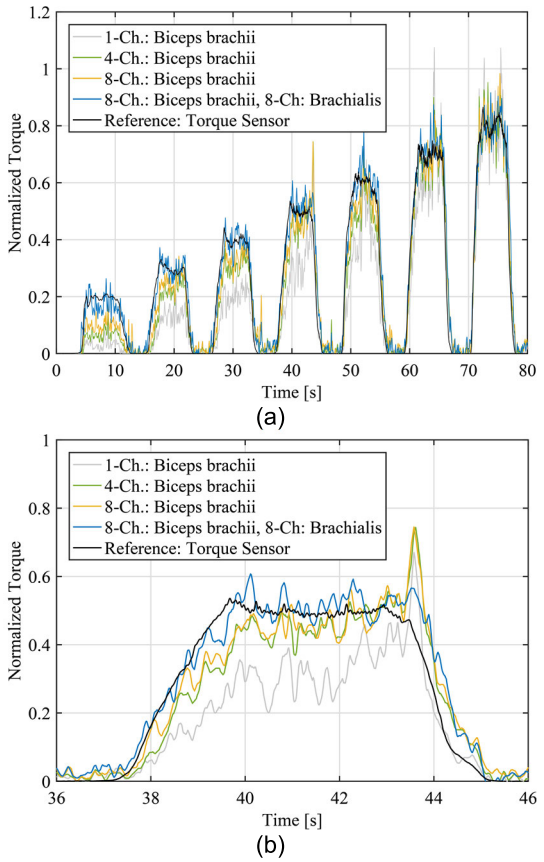

Fig. 9. The results of the validation step (subject 1). (a) Experimental results with respect to the number of electrodes. (b) Torque estimation results for torque level 4. The blue curve is same as in Fig. 8.

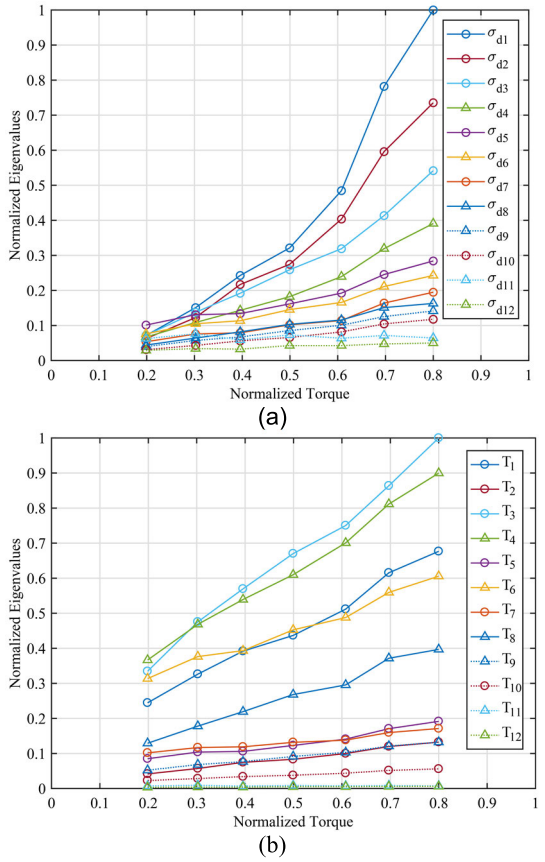

Fig. 11. Relation between eigenvalues and measured torque with respect to subject 1. (a) Normalized and decomposed σ_{d_i}. (b) Normalized and rescaled $T_i = \gamma_i \nu_i$. The circle and triangle markers indicate estimated origins of muscle units in the BB and BR, respectively.

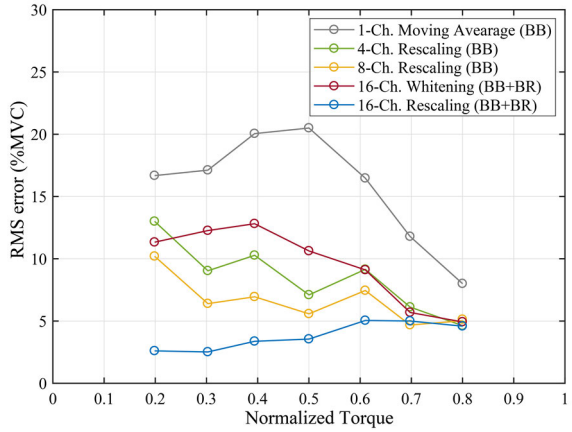

Fig. 10. The results for the RMS errors with respect to different numbers of electrodes and signal processing algorithms. BB: Biceps brachii, BR: Brachialis.

indicate the biceps brachii. As shown in (19), estimation of the origin of the i-th decomposed sEMG component d_i is performed by calculating the magnitude sum of the 1st to 8th elements in the i-th row (i.e., electrodes on the biceps brachii) of the eigenvector matrix $\mathbf{V}$ and comparing it to that of the 9th to 16th elements in the i-th row (i.e., electrodes on the brachialis). If the latter is larger than the former, this implies that d_i originates from the brachialis, and otherwise, it originates from the biceps brachii.

$$\begin{bmatrix} d_1 \\ \vdots \\ d_{16} \end{bmatrix} = \begin{bmatrix} V_{(1,1)} & \cdots & V_{(1,8)} & V_{(1,9)} & \cdots & V_{(1,16)} \\ \vdots & \vdots & \vdots & \vdots & \vdots & \vdots \\ V_{(16,1)} & \cdots & V_{(16,8)} & V_{(16,9)} & \cdots & V_{(16,16)} \end{bmatrix} \begin{bmatrix} m_1 \\ \vdots \\ m_8 \\ m_9 \\ \vdots \\ m_{16} \end{bmatrix} \tag{19}$$

Biceps brachii | Brachialis

According to this estimation, the two strongest muscle units after decomposition (see **Fig. 11**-(a)) originate from the biceps brachii. However, after rescaling, muscle units from the brachialis have almost the same magnitude as those from the biceps brachii (see **Fig. 11**-(b)). For example, in **Fig. 11** of subject 1, σ_{d4} is estimated as the 4th strongest muscle unit after decomposition, but after rescaling, T_4 becomes the 2nd strongest estimated torque level. In most subjects, it is estimated that the 2nd strongest muscle unit after rescaling originates from the brachialis. This result suggests that the rescaling method may restore muscle units in the brachialis to closer to their true magnitudes and implies that sEMG signals

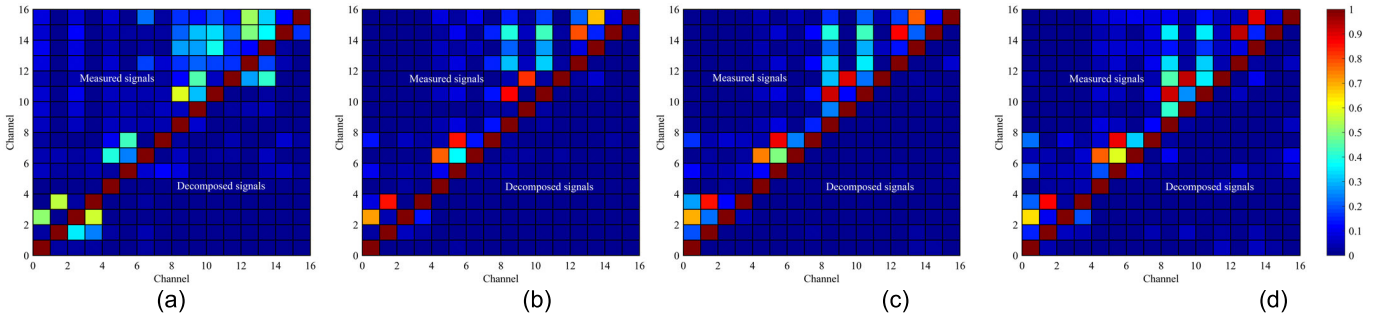

Fig. 12. Correlation coefficients (R^2) among sEMG channels with respect to subject 1. The upper and lower triangles show the correlations among the raw sEMG signals m_i and decomposed sEMG signals d_i, respectively. The eigenvector V is extracted from torque level 4 (50[%] MVC). (a) Torque level 1. (b) Torque level 3. (c) Torque level 5. (d) Torque level 7.

from the brachialis play significant role in accurate torque estimation, although the sEMG signals from the brachialis are relatively small, which belies the significance of the brachialis.

B. Eigenvector and Muscle Units

In this study, eigenvector matrix **V** in (8) is extracted from torque level 4 (50[%] of MVC) and assumed to be a constant matrix. Due to this assumption, the rescaling method can be simply utilized without the need to store an infinite number of eigenvector matrices with respect to every level of muscle activation. This assumption is supported by the experimental results of calculating the correlation among channels with respect to muscle activation level (see **Fig. 12**). In **Fig. 12**, the upper triangle shows the correlation coefficient among the measured sEMG signals m_i, and the lower triangle shows the correlation coefficient among the decomposed sEMG signals d_i. The cross-correlation of the lower triangle remains closer to the zero matrix over the whole torque level, although the eigenvector is extracted from torque level 4. This result suggests that **V** rarely varies with respect to the muscle activation level, and is an almost constant matrix. In other words, **V** can be considered centers of activation of independent muscle units, and these centers are fixed regardless of activation.

From the experimental results in this study, it can be deduced that no muscle unit is newly generated as activation increases. If that happens, **V** has to vary due to the signals from the new muscle unit. In previous studies [37], [38], the neuromuscular compartment in a large muscle group such as the biceps was reported. Regarding these previous studies, it is considered that the invariant property of the muscle units (i.e., the fixed eigenvector **V**) observed in this paper is strongly related to the neuromuscular compartment. However, the variation in the eigenvector matrix **V** should be further investigated under dynamic conditions (i.e., varying muscle length) because the relative locations of the muscle units with respect to the electrodes can change as a muscle contracts. We plan to investigate this topic in future work.

VI. Conclusion

In this study, a high-SNR stochastic sEMG processor with a multichannel electrode was inspired by the whitening method. The principle of the sEMG processor is theoretically introduced, and experimentally verified with respect to multiple muscle human elbow joints. With multichannel electrodes for measuring the activation of deep muscle, muscle unit decomposition, and a linearization algorithm of the rescaling method, the developed sEMG processor shows the most accurate torque estimation result without compromising the time delay problems. From the experimental results, it is considered that the proposed rescaling method with multichannel electrodes is promising and can be applied in robotic rehabilitation engineering to generate rapid and accurate control input signals for robotic devices. To further verify the performance of the developed sEMG processor, in future work, we plan to conduct additional studies with respect to agonist antagonist co-contraction and other multiple muscle joints.

References

[1] R. Mann and S. Reimers, "Kinesthetic sensing for the EMG controlled 'Boston arm,'" *IEEE Trans. Man Mach. Syst.*, vol. MMS-11, no. 1, pp. 110–115, Mar. 1970.

[2] J. Rosen, M. Brand, M. B. Fuchs, and M. Arcan, "A myosignal-based powered exoskeleton system," *IEEE Trans. Syst., Man, Cybern. A, Syst. Humans*, vol. 31, no. 3, pp. 210–222, May 2001.

[3] Y. Na, C. Choi, H. Lee, and J. Kim, "A study on estimation of joint force through isometric index finger abduction with the help of SEMG peaks for biomedical applications," *IEEE Trans. Cybern.*, vol. 46, no. 1, pp. 2–8, Jan. 2016.

[4] B. Hudgins, P. Parker, and R. N. Scott, "A new strategy for multifunction myoelectric control," *IEEE Trans. Biomed. Eng.*, vol. 40, no. 1, pp. 82–94, Jan. 1993.

[5] P. Parker, K. Englehart, and B. Hudgins, "Myoelectric signal processing for control of powered limb prostheses," *J. Electromyogr. Kinesiol.*, vol. 16, no. 6, pp. 541–548, Dec. 2006.

[6] K. Kiguchi, T. Tanaka, and T. Fukuda, "Neuro-fuzzy control of a robotic exoskeleton with EMG signals," *IEEE Trans. Fuzzy Syst.*, vol. 12, no. 4, pp. 481–490, Aug. 2004.

[7] A. M. Dollar and H. Herr, "Lower extremity exoskeletons and active orthoses: Challenges and state-of-the-art," *IEEE Trans. Robot.*, vol. 24, no. 1, pp. 144–158, Feb. 2008.

[8] T. Lenzi, S. M. M. De Rossi, N. Vitiello, and M. C. Carrozza, "Intention-based EMG control for powered exoskeletons," *IEEE Trans. Biomed. Eng.*, vol. 59, no. 8, pp. 2180–2190, Aug. 2012.

[9] R. W. Norman and P. V. Komi, "Electromechanical delay in skeletal muscle under normal movement conditions," *Acta Physiologica Scandinavica*, vol. 106, no. 3, pp. 241–248, Jul. 1979.

[10] L. Li and B. S. Baum, "Electromechanical delay estimated by using electromyography during cycling at different pedaling frequencies," *J. Electromyogr. Kinesiol.*, vol. 14, no. 6, pp. 647–652, Dec. 2004.

[11] G. Howatson, "The impact of damaging exercise on electromechanical delay in biceps brachii," *J. Electromyogr. Kinesiol.*, vol. 20, no. 3, pp. 477–481, Jun. 2010.

[12] T. D. Sanger, "Bayesian filtering of myoelectric signals," *J. Neurophysiology*, vol. 97, no. 2, pp. 1839–1845, Feb. 2007.

[13] N. Hogan and R. W. Mann, "Myoelectric signal processing: Optimal estimation applied to electromyography—Part I: Derivation of the optimal myoprocessor," *IEEE Trans. Biomed. Eng.*, vols. BME–27, no. 7, pp. 382–395, Jul. 1980.

[14] N. Hogan and R. W. Mann, "Myoelectric signal processing: Optimal estimation applied to electromyography—Part II: Experimental demonstration of optimal myoprocessor performance," *IEEE Trans. Biomed. Eng.*, vols. BME–27, no. 7, pp. 396–410, Jul. 1980.

[15] E. A. Clancy and N. Hogan, "Probability density of the surface electromyogram and its relation to amplitude detectors," *IEEE Trans. Biomed. Eng.*, vol. 46, no. 6, pp. 730–739, Jun. 1999.

[16] E. A. Clancy and K. A. Farry, "Adaptive whitening of the electromyogram to improve amplitude estimation," *IEEE Trans. Biomed. Eng.*, vol. 47, no. 6, pp. 709–719, Jun. 2000.

[17] E. A. Clancy, S. Bouchard, and D. Rancourt, "Estimation and application of EMG amplitude during dynamic contractions," *IEEE Eng. Med. Biol. Mag.*, vol. 20, no. 6, pp. 47–54, Nov. 2001.

[18] P. Prakash, C. A. Salini, J. A. Tranquilli, D. R. Brown, and E. A. Clancy, "Adaptive whitening in electromyogram amplitude estimation for epoch-based applications," *IEEE Trans. Biomed. Eng.*, vol. 52, no. 2, pp. 331–334, Feb. 2005.

[19] E. A. Clancy, L. Liu, P. Liu, and D. V. Z. Moyer, "Identification of constant-posture EMG–torque relationship about the elbow using nonlinear dynamic models," *IEEE Trans. Biomed. Eng.*, vol. 59, no. 1, pp. 205–212, Jan. 2012.

[20] C. Dai, B. Bardizbanian, and E. A. Clancy, "Comparison of constant-posture force-varying EMG-force dynamic models about the elbow," *IEEE Trans. Neural Syst. Rehabil. Eng.*, vol. 25, no. 9, pp. 1529–1538, Sep. 2017.

[21] H. Wang et al., "Optimal estimation of EMG standard deviation (EMG σ) in additive measurement noise: Model-based derivations and their implications," *IEEE Trans. Neural Syst. Rehabil. Eng.*, vol. 27, no. 12, pp. 2328–2335, Dec. 2019.

[22] D. Staudenmann and W. Taube, "Brachialis muscle activity can be assessed with surface electromyography," *J. Electromyogr. Kinesiol.*, vol. 25, no. 2, pp. 199–204, Apr. 2015.

[23] J. H. Lawrence and C. J. De Luca, "Myoelectric signal versus force relationship in different human muscles," *J. Appl. Physiol.*, vol. 54, no. 6, pp. 1653–1659, Jun. 1983.

[24] J. S. Bendat and A. G. Piersol, *Random Data: Analysis and Measurement Procedures*, vol. 729. Hoboken, NJ, USA: Wiley, 2011.

[25] A. Boxtel, "Optimal signal bandwidth for the recording of surface EMG activity of facial, jaw, oral, and neck muscles," *Psychophysiology*, vol. 38, no. 1, pp. 22–34, Jan. 2001.

[26] B. Bigland-Ritchie, "EMG/force relations and fatigue of human voluntary contractions," *Exerc. Sport Sci. Rev.*, vol. 9, no. 1, pp. 75–118, 1981.

[27] J. Woods and B. Bigland-Ritchie, "Linear and non-linear surface EMG/force relationships in human muscles. An anatomical/functional argument for the existence of both," *Amer. J. Phys. Med.*, vol. 62, no. 6, pp. 287–299, 1983.

[28] J. Perry and G. A. Bekey, "EMG-force relationships in skeletal muscle," *Crit. Rev. Biomed. Eng.*, vol. 7, no. 1, pp. 1–22, 1981.

[29] J. Vredenbregt and G. Rau, "Surface electromyography in relation to force, muscle length and endurance," in *New Concepts of the Motor Unit, Neuromuscular Disorders, Electromyographic Kinesiology*, vol. 1. Basel, Switzerland: Karger, 1973, pp. 607–622.

[30] A. V. Hill, "The heat of shortening and the dynamic constants of muscle," *Proc. Roy. Soc. London. B, Biol. Sci.*, vol. 126, no. 843, pp. 136–195, Oct. 1938.

[31] H. Chang, G. M. Gu, S. Min, H. Lee, and J. Kim, "Investigation of a tolerable time delay in SEMG-based elbow assistive device," in *Proc. SICE Annu. Conf. (SICE)*, Sep. 2014, pp. 1382–1387.

[32] S. H. Nawab, S.-S. Chang, and C. J. De Luca, "High-yield decomposition of surface EMG signals," *Clin. Neurophysiol.*, vol. 121, no. 10, pp. 1602–1615, Oct. 2010.

[33] J. Woods and B. Bigland-Ritchie, "Linear and non-linear surface EMG/force relationships in human muscles. an anatomical/functional argument for the existence of both," *Amer. J. Phys. Med.*, vol. 62, no. 6, pp. 287–299, 1983.

[34] B. Bigland and O. C. J. Lippold, "The relation between force, velocity and integrated electrical activity in human muscles," *J. Physiol.*, vol. 123, no. 1, pp. 214–224, Jan. 1954.

[35] A. J. Fuglevand, D. A. Winter, and A. E. Patla, "Models of recruitment and rate coding organization in motor-unit pools," *J. Neurophysiology*, vol. 70, no. 6, pp. 2470–2488, Dec. 1993.

[36] D. Farina, C. Cescon, and R. Merletti, "Influence of anatomical, physical, and detection-system parameters on surface EMG," *Biol. Cybern.*, vol. 86, no. 6, pp. 445–456, Jun. 2002.

[37] A. W. English, S. L. Wolf, and R. L. Segal, "Compartmentalization of muscles and their motor nuclei: The partitioning hypothesis," *Phys. Therapy*, vol. 73, no. 12, pp. 857–867, Dec. 1993.

[38] A.-T. Liu et al., "Architectural properties of the neuromuscular compartments in selected forearm skeletal muscles," *J. Anatomy*, vol. 225, no. 1, pp. 12–18, Jul. 2014.